JOURNAL OF GEOPHYSICAL RESEARCH, VOL. 105, NO. C10, PAGES 24,071–24,087, OCTOBER 15, 2000

A mechanism for the generation of wave-driven rhythmic patterns in the surf zone

A. Falqués

Departament de Física Aplicada, Universitat Politècnica de Catalunya, Barcelona, Spain

G. Coco[1] and D. A. Huntley

Plymouth Environmental Research Centre, Institute of Marine Studies, University of Plymouth Plymouth, England, United Kingdom

Abstract. The coupling between topographic irregularities and wave-driven mean water motion in the surf zone is examined. This coupling occurs because the topographic perturbations produce excess gradients in the wave radiation stress that cause a steady circulation. This circulation, in turn, creates a sediment transport pattern that can reinforce the bottom disturbance and may thereby lead to the growth of large-scale bed forms. To investigate this coupling mechanism, the linearized stability problem with an originally plane sloping beach and normal wave incidence is solved in two different cases. First, the breaking line is considered to be fixed, and second, the perturbations in water depth that produce a displacement of the breaker line are accounted for. The first case shows that the basic topography can be unstable with respect to two different modes: a giant cusp pattern with shore-attached transverse bars that extend across the whole surf zone and a crescentic pattern with alternate shoals and pools at both sides of the breaking line showing a mirroring effect. In the second case, the varying breaker line may have a strong influence on the circulation. This is clear for the giant cusp topography whose growth is totally inhibited. In contrast, the morphology and the growth of the crescentic pattern remains almost unchanged.

1. Introduction

The nearshore zone in front of sandy beaches sometimes shows quite regular morphological patterns at length scales well above the length scale of incident wind or swell waves. Giant cusps [*Komar*, 1971], shore-attached oblique/transverse bar systems [*Niedoroda and Tanner*, 1970; *Hunter et al.*, 1979; *Lippmann and Holman*, 1990], crescentic bars [*Bowen and Inman*, 1971] and ridge and runnel systems [*Mulrennan*, 1992] are well-known examples of such features. These patterns are certainly intriguing and have scientific interest in themselves. More importantly, their regularity gives an indication that the large-scale complex dynamics of the surf zone as a whole can be understood in terms of simple physical mechanisms, at least in some circumstances.

These large-scale beach processes, which involve long time-scales have sometimes been related to the presence of low-frequency waves, in particular infragravity edge waves. These waves can be excited by the presence of low-frequency patterns in the external wave forcing [*Bowen and Guza*, 1978; *Holman and Bowen*, 1982]. This is an example of a forced topographic response in which an imposed velocity field creates the underlying topography. However, another possibility is that these patterns can be the result of morphodynamic instabilities of the alongshore uniform equilibrium, an example of free or self-organized behavior of the nearshore dynamical system [*Southgate and Beltran*, 1998]. Of course, it is very plausible that in many circumstances both kind of behaviors will interact on natural beaches.

Since the earlier suggestions by *Sonu* [1968] and the work of *Barcilon and Lau* [1973] and *Hino* [1974], little attention had been paid to nearshore morphodynamic instabilities. In the nineties an increasing interest in this approach developed, and those early investigations have been revisited and extended by *Christensen et al.* [1994], *Deigaard et al.* [1999], *Vittori et al.* [1999], *Falqués* [1991] and *Falqués et al.* [1996a,b]. In addition, the concept of self-organization in the nearshore has been further extended by the work of *Werner and*

[1]Now at Institute of Geophysics and Planetary Physics, Scripps Institution of Oceanography, University of California, San Diego, La Jolla.

Copyright 2000 by the American Geophysical Union.

Paper number 2000JC900100.
0148-0227/00/2000JC900100$09.00

Fink [1993] and *Coco et al.*, [1999a, b] by using cellular automata methods.

Morphodynamic instabilities arise from the coupling that sediment transport induces between the small perturbations on a reference uniform bottom topography and the disturbances thereby produced on water motions. In the case of normal wave incidence, where there is no longshore current, this coupling can occur through the perturbation that the bed forms cause on the incident wave field. Basically, the shoals and the troughs cause wave energy redistribution, variations in the breaking point, wave refraction, reflection, and diffraction, which produce, in turn, a radiation stress distribution that is no longer in equilibrium with the setup/setdown, and a steady circulation is created. We will refer to this interaction as bed-surf interaction.

When there is a significant longshore current, the deflection that the bed forms produce on the current is another source of morphodynamic interaction. This mechanism is responsible for the formation of free bars in rivers and can also be important in the nearshore environment in case of currents generated by tides, by wind stress, or by river discharge. We will refer to it as bed-flow interaction. For wave-driven longshore currents this effect is usually mixed with the bed-surf interaction. However, from a conceptual point of view, bed-flow interaction is worth investigating in isolation [*Falqués et al.*, 1996a and *Falqués et al.*, 1996b] suggest that the bed-flow mechanism can be dominant under some circumstances. This is quite satisfactory since bed-flow effects are much easier to deal with than bed-surf interaction, which is based on the complex processes that waves undergo within the surf/shoaling zone.

Normal wave incidence is assumed in the present paper to avoid a mean longshore current. A satisfactory understanding of each of the individual processes, bed-flow and bed-surf, in isolation is convenient before dealing with the general situation of oblique wave incidence. As far as we know, instability in case of normal wave incidence is essentially unexplored. For instance, the model of *Christensen et al.* [1994] could not deal with the case of $\theta_b = 0$. Apparently, *Hino* [1974] did some numerical experiments with normal incidence. However, even though his results were promising, a lack of a systematic investigation by both numerical and analytical tools is apparent. More recently, *Vittori et al.* [1999] proposed a morphodynamic instability mechanism resulting in the formation of crescentic patterns. Such an approach considers normally incident waves and results in the appearance of rhythmic features offshore of the breaking area so that the direct influence of a moving breaking line is not considered.

The purpose of the present paper is to present a first detailed investigation of bed-surf interaction as a source of morphodynamic instability. In fact, this paper is the natural continuation of *Falqués et al.* [1999a] who showed that there were not purely hydrodynamic instabilities in the case of normal incidence unless wave-current or bed-surf interactions were taken into account. We will concentrate here on a single bed-surf effect: wave energy redistribution in the surf zone which is believed to be the major source of bed-surf interaction at an initial stage. This analysis shows that even with this rather simplified modeling, morphodynamic instability indeed develops and produces bed forms that compare well with features that can occur on natural beaches. Furthermore, this study suggests some interesting links between morphological patterns and sediment transport modes. The effect of the variation of the breaking point due to the bed forms, always disregarded in previous studies concerning morphodynamic instabilities in the nearshore region [*Hino*, 1974; *Christensen et al.*, 1994; *Vittori et al.*, 1999], will be also investigated, and the importance of such a localized effect will be considered in detail. On the other hand, wave refraction will be neglected here and its effect left for further research. Also, the present study is restricted to the case of non-barred beaches and to only the initial growth of the perturbations.

In section 2 we present the theoretical setting of morphodynamic stability. In section 3 we give some general properties of the instability and investigate the physical mechanisms. This is done by analytical tools and by considering an idealized situation. In section 4 we present numerical simulations under the hypothesis of a fixed breaking line. In section 5 we present numerical experiments in case of more realistic conditions that include a varying breaking line. In section 6 we give a brief summary, some discussion, and a comparison with natural morphological patterns. Three appendixes are included, one on the sediment transport parameterisation, the second on some mathematical developments, and the third on the parameterization of the moving breaking line.

2. Governing Equations and Stability Analysis

2.1. Governing Equations

We consider a rectilinear beach with a shoreline given by the y axis and with a topography given by $z = z_b(x, y, t)$, where x is the cross-shore coordinate and z is the vertical one (positive upward, see Figure 1). The two-dimensional horizontal nearshore hydrodynamics on timescales larger than the incident waves proceed from depth-averaged momentum and mass conservation and read

$$\frac{\partial v_i}{\partial t} + v_j v_{i,j} = -g z_{s,i} - \frac{1}{\rho D}(\tau_i + S_{ij,j}) + \frac{1}{D}[\nu D(v_{i,j} + v_{j,i})]_{,j} \qquad i = 1, 2 \tag{1}$$

$$\frac{\partial D}{\partial t} + (D v_j)_{,j} = 0 \tag{2}$$

Here $\mathbf{v} = (v_1, v_2)$ is the depth-averaged horizontal ve-

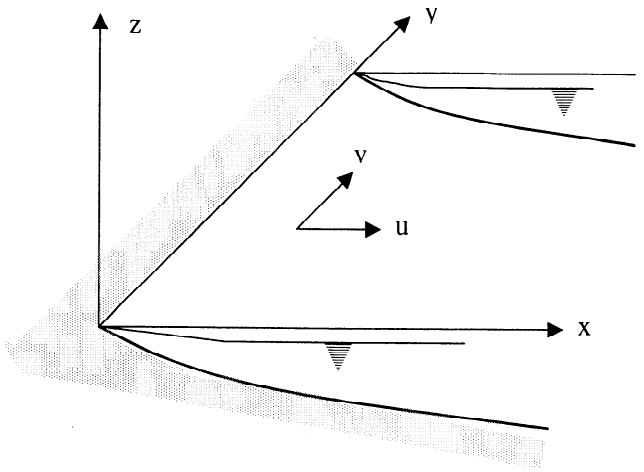

Figure 1. Sketch of the geometry and coordinate system.

Figure 1:

locity, $x_1 = x$, $x_2 = y$, and repeated indexes are assumed to be summed. The derivative with respect to x_i has been indicated by the subindex i. The total depth is $D = z_s - z_b$, where $z_s(x, y, t)$ stands for the free surface elevation. The bottom shear stress is $\boldsymbol{\tau}$, and the water density is ρ. The lateral mixing from wave breaking turbulence is parameterized by means of the eddy viscosity coeficient $\nu(x)$. The forcing from incident waves is given by the radiation stresses, which read

$$S_{ij} = [\frac{k_i k_j}{k^2} + \frac{1}{2}\delta_{ij}]E \qquad i,j = 1,2 \tag{3}$$

where $\mathbf{k}$ and E are the wave number and the energy of incident waves, respectively [*Horikawa*, 1988]. Since we are dealing with shallow water waves, the phase and the group celerities are assumed to coincide approximately, $c_p = c_g = c$. The morphological evolution is given by the sediment conservation equation

$$\frac{\partial z_b}{\partial t} + q_{j,j} = 0\,, \tag{4}$$

where $\mathbf{q}(\mathbf{v}, z_b)$ is the horizontal sediment flux vector.

2.2. Basic state

We now consider regular incident wind or swell waves approaching the beach normally with energy distribution $E = E_0(x)$ and look for a basic undisturbed state, which is a steady and motionless solution of (1), (2), and (4), that is,

$$v_1 = v_2 = 0 \quad , \quad z_s = \zeta_0(x) \quad , \quad z_b = -d_0(x) \tag{5}$$

The radiation stresses will be of the form

$$S_{xx} = \frac{3}{2}E_0(x)\,, \quad S_{yy} = \frac{1}{2}E_0(x)\,, \quad S_{xy} = 0\,. \tag{6}$$

Furthermore, we will assume that both the bottom shear stress and the sediment flux are proportional to some power of the mean flow velocity. Therefore, since $\mathbf{v} = 0$, the bottom friction and the sediment flux will vanish: $\boldsymbol{\tau} = 0$, and $\mathbf{q} = 0$. As a result, the cross-shore component of (1) reads

$$g\frac{d\zeta_0}{dx} = -\frac{3}{2\rho}\frac{1}{d_0 + \zeta_0}\frac{dE_0}{dx}\,, \tag{7}$$

with the other governing equations being verified. Thus the basic undisturbed state is defined as a steady setup/setdown of the mean water level given by $z_s = \zeta_0(x)$ over a fixed topography without mean motion.

2.3. Linear stability equations

Any departure from the basic planar topography will produce a modification of the incident wave field. The wave energy distribution will change, and as a result, the setup and the setdown of the basic state, $\zeta_0(x)$, will not be in equilibrium any longer, and a mean flow will thus be generated. This flow will carry sediments so that the initial topographic disturbance will evolve. A morphodynamic loop will thus be formed, and if a positive feedback occurs, a new topography coupled to a horizontal circulation will develop in time. To look at this possibility, a small perturbation will be assumed on the topography and on the mean free surface:

$$\begin{aligned} z_b(x,y,t) &= -d_0(x) + h(x,y,t) \\ z_s(x,y,t) &= \zeta_0(x) + \eta(x,y,t)\,, \end{aligned} \tag{8}$$

and a small horizontal mean flow,

$$\mathbf{v} = (u(x,y,t), v(x,y,t))\,, \tag{9}$$

will be assumed as well. We will look at the dynamics of these small perturbations by linearizing the governing equations (1), (2), and (4) with respect to them.

A difficult and crucial point is how this disturbance will affect the incident wave field. In a saturated surf zone this will be basically through three effects: wave energy redistribution, wave refraction by depth variations and currents, and the modification of the breaking point by growing shoals and pools at the breaking line. Both thewave refraction and the modification of the breaking point are first-order effects (with respect to the perturbations). The influence of a varying breaking line will be analyzed in detail as will the importance of such a "localized" effect on the growth of morphological patterns. On the other hand, the effect of wave refraction, because diffused over much wider areas, will be assumed to be comparatively small, at least in a linear analysis, with respect to the other effects and will be neglected in this study. Thus we will keep waves approaching normally to the shore, while their energy will suffer small modifications because of depth variations. For this purpose [see also *Falqués et al.*, 1999a], we will assume that wave energy in the nearshore is a known function of the total depth:

$$E = E(D)\,. \tag{10}$$

This allows us to describe one source of coupling between morphology and waves in a quite simple manner.

How wave refraction affects this mechanism is left for future research. Note that (10) is not valid in the case of barred beaches. Thus we will hereinafter assume a planar beach profile. Equation (10) can easily be determined for a saturated surf zone, where

$$E = \frac{1}{8}\rho g \gamma_b^2 D^2 \tag{11}$$

is usually assumed with $\gamma_b \sim 1$ being a breaking index. The Green's law for wave amplitude in the shoaling zone is also in accordance with the form of (10) [*Mei*, 1989].

Sediment transport parameterization is another important point. The sediment flux is usually parameterized as being proportional to some power m of the mean flow and the wave orbital velocity. Since there is no flow in the basic state, the sediment transport in the perturbed state will be proportional to the power m of $\mathbf{v}$ which is first order. Then, if $m > 1$, the linearized problem would have no sediment transport. Therefore we will assume that $m = 1$ in our linear analysis, and we will leave for future research the nonlinear problem, checking the robustness of the instability mechanism to the choice of m. Thus we will assume that

$$\mathbf{q} = \hat{\alpha}(x)\mathbf{v} - \hat{\gamma}(x)\nabla h\,. \tag{12}$$

This linear parameterization of sediment transport can be interpreted as the sediment's being stirred by wave motion and then advected by the mean current. Thus $\alpha(x)$ is a wave stirring coefficient, which is expected to have a cross-shore gradient (see Appendix A). Furthermore, because of both wave oscillations and wave-breaking turbulence, any bump superimposed on the nearshore sea bottom will be potentially smoothed out if no positive feedback occurs into the water motion. This is parameterized through a morphodynamic diffusion coefficient $\gamma(x)$ in (12).

Bottom shear stress will also be parameterized as being proportional to the mean flow through a coefficient that depends on the wave orbital velocity U_0 :

$$\frac{\tau_{bx}}{\rho D} = \hat{\mu}_x u \quad \frac{\tau_{by}}{\rho D} = \hat{\mu}_y v\,, \tag{13}$$

where $\hat{\mu}_x = 2\hat{\mu}_y = 4c_f U_0/(\pi D_0)$ and where, in the surf zone, $U_0 = (\gamma_b/2)\sqrt{gD_0}$ [*Horikawa*, 1988]. Here c_f is the drag coefficient that relates the instantaneous bottom shear stress to the squared instantaneous velocity $\tau = \rho c_f v^2$. The momentum diffusion in the surf zone will be parameterized as

$$\nu(x) = Nx\sqrt{gD} \tag{14}$$

and as an exponential decay beyond the breaking line. The constant N is estimated to range between 0.01 and 0.06 [*Bowen and Inman*, 1972] although smaller values have also been suggested [*Longuet-Higgins*, 1970a, b].

Now we are going to introduce a scaling. The width of the surf zone, X_b, is chosen as the horizontal length scale and a vertical length scale βX_b will be introduced where β is some mean slope of the basic topography $O(dd_0/dx) = \beta$. An arbitrary velocity scale U is also considered. The natural timescale for hydrodynamics is then X_b/U. However, morphological evolution is much slower, with a timescale T that will be defined later. We will have $\epsilon = (X_b/U)/T \ll 1$. Then we will define the nondimensional variables as:

$$(x,y) = X_b(x',y')\,, \quad h = \beta X_b h'\,, \quad D_0 = \beta X_b D_0'$$

$$(u,v) = U(u',v')\,, \quad \eta = \frac{U^2}{g}\eta'\,, \quad t = Tt'\,.$$

Hereinafter primes will be dropped for simplicity. Then the linearized nondimensional form of the governing equations (1) and (2) in the surf zone will read

$$\epsilon\frac{\partial u}{\partial t} + \mu_x u + (1+\frac{3}{8}\gamma_b^2)\frac{\partial \eta}{\partial x} - \mathcal{V}_x = \frac{3}{8}\frac{\gamma_b^2}{F^2}\frac{\partial h}{\partial x}\,, \tag{15}$$

$$\epsilon\frac{\partial v}{\partial t} + \mu_y v + (1+\frac{1}{8}\gamma_b^2)\frac{\partial \eta}{\partial y} - \mathcal{V}_y = \frac{1}{8}\frac{\gamma_b^2}{F^2}\frac{\partial h}{\partial y}\,, \tag{16}$$

$$\epsilon\frac{\partial}{\partial t}(F^2\eta - h) + \frac{\partial}{\partial x}(D_0 u) + \frac{\partial}{\partial y}(D_0 v) = 0\,, \tag{17}$$

where a Froude number $F = U/\sqrt{g\beta X_b}$ has been introduced and $\mu_x = \hat{\mu}_x X_b/U$ and $\mu_y = \hat{\mu}_y X_b/U$ have been defined. The nondimensional coefficients μ_x and μ_y depend on the drag coefficient c_f through $r = c_f/\beta$, which will be adopted as the frictional parameter for our simulations [see *Falqués et al.*, 1996a]. Notice that the same equations will be valid out of the surf zone, but, since there are no perturbations on the radiation stress, γ_b must be substituted by 0. The momentum diffusion terms read

$$\mathcal{V}_x = \frac{2}{D_0}\frac{\partial}{\partial x}(\nu D_0\frac{\partial u}{\partial x}) + \nu\frac{\partial}{\partial y}(\frac{\partial u}{\partial y} + \frac{\partial v}{\partial x})$$

$$\mathcal{V}_y = \frac{1}{D_0}\frac{\partial}{\partial x}(\nu D_0(\frac{\partial u}{\partial y} + \frac{\partial v}{\partial x})) + 2\nu\frac{\partial^2 v}{\partial y^2}\,.$$

Equations (15)-(16) describe the linearized momentum balance only in the case of a fixed breaking line. As shown in Appendix C, a moving breaking line changes the linearization of the cross-shore momentum balance.

To scale the sediment conservation equation (4), we first define a nondimensional wave-stirring coefficient:

$$\hat{\alpha}(x) = \bar{\alpha}\alpha(x)\,,$$

where $\alpha(x)$ is now order one. By carrying out the scaling of (4) the coefficient $UT\bar{\alpha}/\beta X_b$ appears in front of $\alpha(x)$ in the divergence of the sediment flux. Therefore, if we want significant morphological changes during one time unit, we must choose a morphological timescale

$$T = \beta\frac{X_b^2}{U\bar{\alpha}}\,. \tag{18}$$

Then, from (4) the bottom evolution equation becomes

$$\frac{\partial h}{\partial t} + \frac{\partial}{\partial x}(\alpha u) + \frac{\partial}{\partial y}(\alpha v) = \frac{\partial}{\partial x}(\gamma\frac{\partial h}{\partial x}) + \frac{\partial}{\partial y}(\gamma\frac{\partial h}{\partial y})\,, \tag{19}$$

where $\gamma = \hat{\gamma}T/X_b^2$.

Now, in case of a fixed breaking line the linear stability analysis proceeds in its standard way by assuming alongshore periodic perturbations of the form

$$[u(x,y,t), v(x,y,t), \eta(x,y,t), h(x,y,t)] = \Re e\{e^{\sigma t+iky}[\hat{u}(x), \hat{v}(x), \hat{\eta}(x), \hat{h}(x)]\}, \quad (20)$$

where $2\pi/k$ is its alongshore wavelength and σ is its growth rate. By inserting this form of the solution into the system of the governing equations (15), (16), (17) and (19) an eigenproblem is obtained, where σ is the eigenvalue and $(\hat{u}(x), \hat{v}(x), \hat{\eta}(x), \hat{h}(x))$ is the eigenfunction. Its structure is the same as that of (15), (16), (17) and (19) but with the substitutions of $\partial/\partial t$ by σ and $\partial/\partial y$ by ik.

A spectral numerical technique based on the use of rational Chebyshev functions has been applied in order to solve the eigenvalue problem posed by the linear stability analysis. This method has already been successfully applied to other morphodynamical models (see, for instance, *Falqués et al.* [1996a, b]) where a description of the technique can also be found) and allows for the determination, for a given wavenumber, of as many eigenvalues as the number of discretization points. The numerical model that solves the present eigenproblem is called *morfo13*. The relevant morphodynamic instability modes have real σ in this case. This means a growth (if $\sigma > 0$) in place without migration. The model is also able, however, to describe purely hydrodynamic modes like edge waves. In this case the imaginary part of σ is the frequency, and it gives the alongshore phase speed. The relevant extension of the model, taking into account the effect of a moving breaking line, is described in detail in Appendix C.

3. Analysis of the Instability Mechanism

In sections 4 and 5, the use of the numerical model *morfo13* will show that morphodynamic instability indeed develops, and the properties of such a process will be explored for quite realistic conditions. However, the use of analytical tools, when possible and perhaps in very idealized situations, gives a better understanding of the outputs of the numerical models and a higher confidence in them. This section is devoted to some analytical developments concerning the bed-surf interaction.

3.1. Bottom Evolution Equation

A very useful tool for analyzing morphodynamic instabilities is a bottom evolution equation where only the cross-shore flow component is involved [*Falqués et al.*, 1996a]. This form of equation can easily be obtained by substituting $\partial v/\partial y$ from the mass conservation equation (17) into the sediment conservation equation (19). Since the morphologic evolution is much slower than the fluid motions, we can safely consider $\epsilon = 0$ in this section. Then the bottom evolution equation will read

$$\frac{\partial h}{\partial t} - \frac{\partial}{\partial x}(\gamma\frac{\partial h}{\partial x}) - \frac{\partial}{\partial y}(\gamma\frac{\partial h}{\partial y}) = -u\,\alpha\,\frac{d}{dx}\ln(\frac{\alpha}{D_0}). \quad (21)$$

The conditions leading to the instability are immediately found from (21). The growth of any bed form requires $\partial h/\partial t > 0$, where $h > 0$, and $\partial h/\partial t < 0$, where $h < 0$. In the linear theory each of these conditions implies the other. So, let us examine when the first condition occurs. The second and the third terms on the left-hand side are diffusive so that they play just a damping role, and any instability will be related to the right-hand term. Thus, since $\alpha > 0$, instability requires that

$$u\,\frac{d}{dx}\ln(\frac{\alpha}{D_0}) < 0, \quad (22)$$

where $h > 0$, that is, over the shoals. This means that the shoals grow if the cross-shore flow opposes the gradient of the $\alpha(x)/D_0(x)$ function. In other words, if the stirring function increases seaward faster (slower) than the water depth, the growth of bed forms needs a shoreward (seaward) flow over the shoals.

This can be understood as follows. Assume first a constant α. A seaward flow over a sloping beach has to converge in order to preserve mass, as the depth is increasing in the direction of the water motion. Since α is constant, this implies a convergence of sediments and therefore sedimentation. Assume now a constant depth but an increasing wave stirring α and assume again a seaward flow. Its divergence will now vanish. However, given a control volume, the sediment concentration will be smaller at its shoreward side than at its seaward side. Therefore more sediment will go out than will enter the control volume, so erosion will occur. Thus we get two counteracting effects, one related to the gradients in the depth, $D_0(x)$, and the other related to the gradients in the stirring function, $\alpha(x)$.

To conclude this stability analysis, we now need to know, for any given topographic pattern, whether the cross-shore flow will be seaward or shoreward over the shoals. This requires solving the flow equations (15), (16) and (17) for a given bottom perturbation h, that is, the "flow over topography problem" (FOT problem).

3.2. FOT Problem

In this section and in section 3.3 the variations of the breaker line will be disregarded. We will assume that the bottom perturbation and the flow related to it are alongshore periodic; that is, we will assume the form given by (20). Lateral momentum mixing will be neglected here since it is not essential for the instability mechanism. Its effects will be investigated numerically in section 5. Also, the quasi-steady approximation, $\epsilon = 0$, will be adopted as in the section 3.1. For simplicity the hats on u, v, η and h are dropped. With all these assumptions, and defining the parameters

$$m = \frac{1}{8}\gamma_b^2 \quad s = \frac{\gamma_b^2}{8F^2},$$

the flow equations (15), (16) and (17) read

$$\mu_x u + (1+3m)\frac{\partial \eta}{\partial x} = 3s\frac{\partial h}{\partial x} \tag{23}$$

$$\mu_y v + ik(1+m)\eta = iksh, \tag{24}$$

$$\frac{\partial}{\partial x}(D_0 u) + ikD_0 v = 0. \tag{25}$$

Substitution of v and η from (25) and (24) into (23) leads to a single equation in u:

$$\frac{\partial}{\partial x}\left[\frac{\mu_y}{D_0}\frac{\partial}{\partial x}(D_0 u)\right] - \frac{1+m}{1+3m}\mu_x k^2 u = -\frac{2s}{1+3m}k^2\frac{\partial h}{\partial x}. \tag{26}$$

As for the flow equations (15), (16) and (17), (26) is only valid within the surf zone. However, (26) works outside the surf zone if we substitute γ_b with 0; That is, if we make $s = m = 0$. Appropriate boundary conditions are a vanishing mean cross-shore flow at the shoreline and far offshore, $u(0) = u(\infty) = 0$.

An interesting property of the solutions of the FOT equation (26) is that they satisfy the inequality

$$\int_{x_1}^{x_2} D_0 u\frac{\partial h}{\partial x}\,dx > 0 \tag{27}$$

where x_1 and x_2 are any cross-shore positions within the surf zone with $u(x_1) = 0$ and either $u(x_2) = 0$ or $x_2 = 1$ (breakpoint). This can be shown by means of an integral identity, which is obtained by integration by parts after multiplying (26) by $D_0 u$. The mathematical details are left for Appendix B. Essentially, this inequality means that a decrease of the bottom slope with respect to the equilibrium ($\partial h/\partial x > 0$ makes $-\partial z_b/\partial x$ smaller) produces an offshore flow, $u > 0$ (on average). This can be understood because a smaller bottom slope induces a smaller cross-shore gradient in radiation stress so that the equilibrium setup becomes too large and induces a seaward current. A priori, however, this is not so straightforward since there is also a contribution from free surface variations, which are implicitly taken into acccount.

3.3. The Instability Mechanism in a Simple Case

We now turn to a simple idealized situation where morphodynamic instability can be predicted by the analytical tools developed in sections 3.1 and 3.2. The basic assumption now is that α/D_0 is a monotonically increasing function. This may be realistic in the surf zone but not beyond the breaking line. However, this case provides an example of how bed-surf interaction can indeed lead to morphodynamic instability. More realistic situations will be dealt with in sections 4 and 5 by means of numerical experiments. The example we now describe provides some confidence in the numerical model set up to solve the instability equations in realistic conditions.

In this study we assume a shoal with a monotonically decreasing amplitude seaward, $\partial h/\partial x < 0$. Then, according to (27) the cross-shore velocity is shoreward ($u < 0$) everywhere on the shoal. Indeed, assume that there was a cross-shore location $x = x_3$, where $u(x_3) > 0$. Then, by continuity, there would exist x_1' and x_2' such that $\infty \geq x_2' \geq x_3 > x_1' \geq 0$ such that $u(x_1') = u(x_2') = 0$ and $u(x) > 0$ for all $x_2' > x > x_1'$. In this case, (27) would not be satisfied. Therefore such a shoal would produce a shoreward current (and of course, because of the alongshore periodicity, a seaward current in the troughs between shoals). Then, according to the bottom evolution equation (21), since α/D_0 is an increasing function, an inshore flow over the shoals will produce a growth of such shoals (see Figure 2). Thus the motionless equilibrium on a plane sloping beach would be unstable with respect to this kind of topographic perturbations. Of course, this depends on the basic assumption of an ever increasing α/D_0 function, which is not realistic. By numerical simulation we will see that the topographic and flow patterns emerging

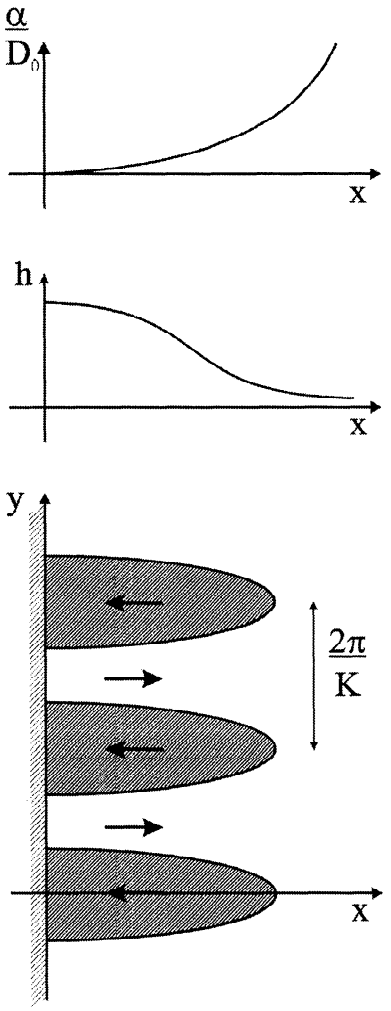

Figure 2. Sketch of the bed-surf instability mechanism in the idealized case of a monotonically increasing α/D_0 function.

from the instability are very sensitive to the sediment transport parameterization.

4. Numerical Simulation With a Fixed Breaking Line

The previously described eigenvalue problem has been here solved numerically in order to assess the sensitivity of the morphodynamic instabilities and their alongshore spacing to parameters such as the bottom friction, the eddy viscosity, and the morphodynamic diffusion. The numerical model has also been used to evaluate the sensitivity of the results to the quasi-steady hypothesis and the convergence of the numerical solution for a different number of discretization points. Finally, the dependence of the results on the way the stirring function is parameterised in the sediment transport formulation has been carefully analyzed. A plane sloping beach has been assumed through all the numerical simulations.

Physically realistic ranges of parameter values have been used. The parameter related to the bottom friction, r, has been varied between 0.01 and 0.5, and that representing the eddy viscosity, N, has been varied between 0.001 and 0.02. For the morphodynamic diffusion parameter γ a profile changing with the cross-shore velocity gradients has been considered with a maximum value ranging between 0.01 and 0.1, chosen at the beginning of the simulation. Values of these parameters from out of the defined ranges have sometimes been used in order to understand their effect and importance for the growth of the instability. The simulations show robustness toward all the parameters concerning hydrodynamic and morphodynamic behavior but a very strong dependence on the form of the stirring function α used in the sediment transport formulation. For this reason, results will be analyzed separately for a series of qualitatively distinct forms of the stirring function $\alpha(x)$.

4.1. Crescentic Bar Pattern

For simplicity the first case analyzed is a stirring function $\alpha(x)$ quadratically increasing from a small shoreline value to the breaking line. Seaward of the surf zone, the stirring function is kept constant and equal to the value at the breaking line (simulations have also been run with an exponential decrease beyond the breaking line, but the results are not significantly affected by such a change). Figure 3 shows a typical growth rate curve (the real part of the frequency σ) for a defined and realistic set of the parameters. In general, results are quite robust and indicate an along-shore spacing of the resulting features between 3 and 5 times the width of the surf zone. Significantly different values are obtained only when the input parameters are extended toward non-realistic values. A feature that all these simulations as well as most of the ones that will be shown in the following sections, have in common is the lack of other modes displaying unstable wavenumbers ($\sigma > 0$). Other modes are obviously present, but they are all characterized by negative growth rates unless unrealistically low values for the parameters related to the damping of the topography (bed friction and diffusivity) are chosen.

The typical perturbation pattern and the related flow pattern are shown in Figure 4. Because of the linear analysis, the amplitude of the topographic disturbance is arbitrary. A 3-D view is given in Figure 5 that clearly shows the presence of periodic features, resembling what in the literature have been defined as crescentic bars [*Bowen and Inman*, 1971; *Lippmann and Holman*, 1990] , around the breaking line. A form of "mirroring effect" offshore of the breaking line is also present such that opposite to deposition, an area of erosion is present and viceversa. In agreement with the theoretical analysis of section 3, the flow pattern is such that onshore flow is present over the shoals, and offshore flow is present over the troughs within the surf zone, where α/D increases. Beyond the breaking line the opposite occurs since α/D decreases.

Simulations have also been performed with a sediment transport parameterization that is very similar to the approach given by *Bowen* [1980] and *Bailard* [1981]. As shown in Appendix A, this results in a stirring coefficient and in a morphodynamic diffusion increasing inside the surf zone as offshore distance to a power of $3/2$ and $5/2$, respectively, and decreasing out of the surf zone to a power of $-9/4$ and $-15/4$, respectively. The pattern obtained through this simulation is qualitatively similar to that for the quadratic function of offshore distance. The only difference is that the growth rate is smaller than that shown in Figures 4 and 5. The use of such exponents should not be considered as an attempt to obtain more realistic results but an attempt to indicate the robustness of the results and the possible link to already accepted approaches.

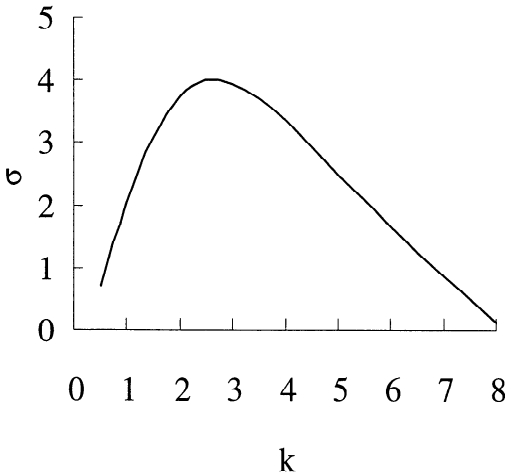

Figure 3. Nondimensional growth rate σ as a function of nondimensional alongshore wavenumber k in the case of $r = 0.1, N = 0.01, \gamma = 0.02$, and $\alpha(0) = 0.1$

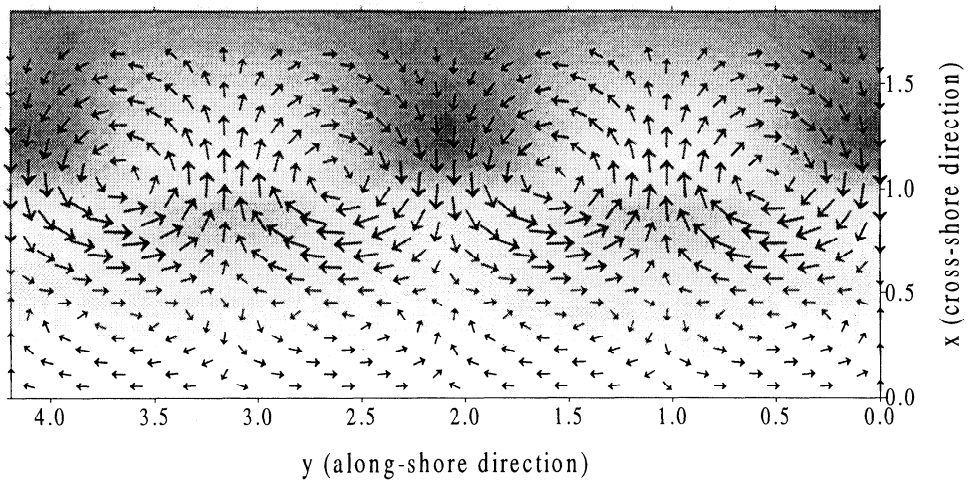

Figure 4. Topographic perturbation and flow pattern ($k = 3.0, r = 0.5, N = 0.01, \gamma = 0.02$, and $\alpha(0) = 0.1$). Shoals are white, and deeper areas are shaded. The shoreline is at $x = 0.0$ and the breaking at $x = 1.0$.

4.2. Giant Cusp Pattern

So far, we have considered only a sediment transport stirring function $\alpha(x)$, which increases through the surf zone. The use of a constant value of α throughout the whole cross-shore section does not affect the process generating the instability, and compared to the previously analyzed case, results seem to indicate a higher variability of the wavelength such that the spacing of the bed forms may vary between 2 and 8 times the width of the surf zone (see, e.g. Figure 6).

The difference between an increasing $\alpha(x)$ and a constant $\alpha(x)$ is much more evident when the bottom perturbation and the flow pattern are analyzed (Figure 7). For constant α the shape of the bottom perturbation now extends to the shoreline and is not restricted to the region around the breaking line. Also, the mirroring effect present for the case of a varying stirring coefficient is not now present, as can be clearly seen from the 3-D view given in Figure 8. The flow (Figure 7) is offshore over the shoals so that the final pattern, for both flow and topography, is very similar to that related to rip currents and giant cusps as reported by different authors [*Shepard*, 1963; *Komar*, 1971]. This is again in accordance with the theoretical analysis in section 3 since α/D is now decreasing through the surf zone. The case of constant α does not present any other mode characterized by a positive growth.

As an example of a stirring coefficient $\alpha(x)$ that is decreasing from the shoreline, an exponentially decaying form has also been studied. As discussed in Appendix A, such runs might simulate conditions where reflection at the shoreline or infragravity motions are predominant. The morphology resulting from such sim-

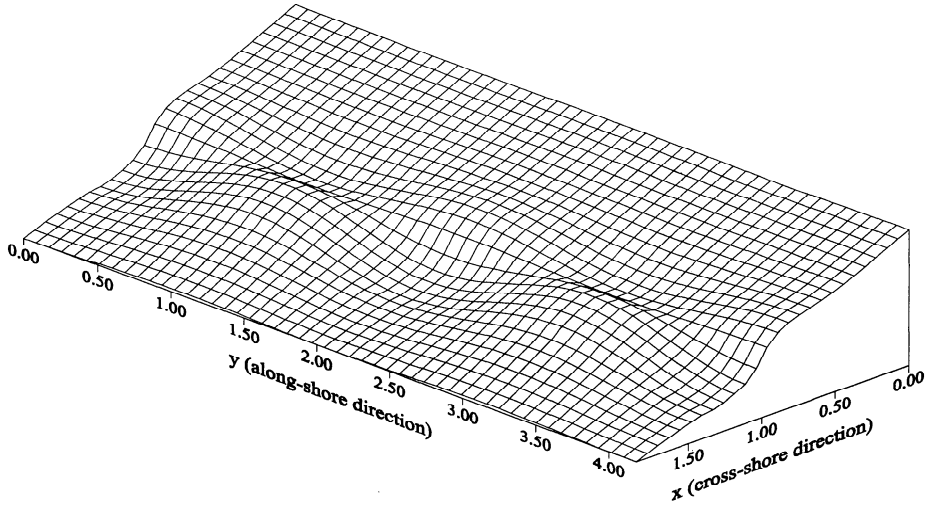

Figure 5. A 3-D view of the topographic perturbation (basic slope and perturbation amplitude have chosen arbitrarily) for $k = 3.0, r = 0.5, N = 0.01, \gamma = 0.02$, and $\alpha(0) = 0.1$. The shoreline is at $x = 0.0$, and the breaking line is at $x = 1.0$.

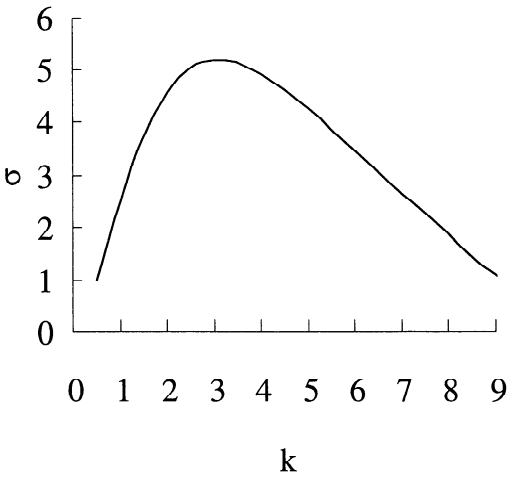

Figure 6. Nondimensional growth rate σ as a function of nondimensional alongshore wavenumber k in the case of $r = 0.1, N = 0.01, \gamma = 0.02$, and $\alpha(x) = \text{const}$.

ulations is always that previously associated with the "giant cusps" patterns (Figure 7), and the only effect of increasing the power of the exponential decay is a shift of the maximum of the perturbation toward the shoreline.

5. Numerical Simulations Including Breaking Line Variation

The introduction of a moving breaking line, described in detail in Appendix C, has a significant effect on the formation of morphological patterns in the nearshore region. Not only the growth rates but also the existence of the patterns can significantly depend on the inclusion of a moving breaking line in the model. For this reason the flow patterns produced by the topographic perturbations previously obtained have been considered in order to check if a further finite development is possible or if any growth of the features is prevented. The study of the wave-driven flow over a given small topographic perturbation has been achieved by solving the linear FOT problem (equation 26) for a fixed h.

5.1. Crescentic Bar Pattern

The influence of a varying breaker on the crescentic bar pattern appears to be limited. Growth rates slightly decrease, but the pattern appears to be very stable. A sensitivity analysis has been performed in order to check the variations in the growth rates with changing parameters. The results, shown in Figure 9, clearly indicate the presence of a maximum characterized by a wavelength around twice the width of the surf zone. In particular, Figure 9 (a), shows the variations induced by using different values of the friction parameter r. Evidently such changes only affect the maximum growth rate but not the wavelength of such a maximum. Furthermore, in reality the value of r should be considered quite constant, and a value of 0.1 seems to be acceptable. Variations in the momentum diffusion N and morphodynamic diffusion γ have relative importance in the growth of the instability (Figures 9b and 9c respectively). As expected, the higher their values the smaller the perturbation growth rates. Another interesting result that has revealed its consistency throughout all the simulations, with and without the inclusion of the breaking line effect, concerns the quasi-steady hypothesis. The model, in fact, allows this hypothesis to

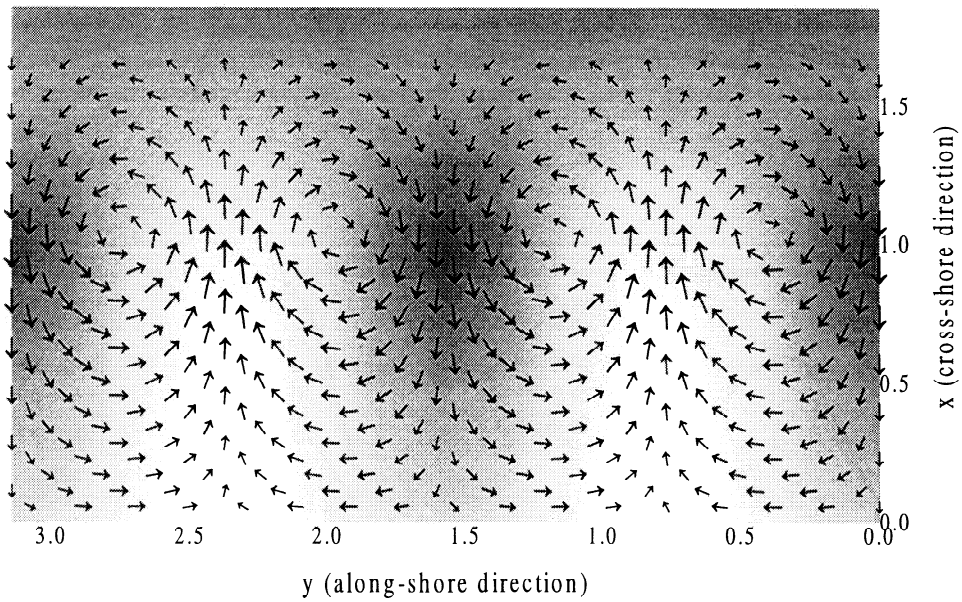

Figure 7. Topographic perturbation and flow pattern ($k = 3.0, r = 0.5, N = 0.01, \gamma = 0.02$, and $\alpha(x) = \text{const}$.). Shoals are white, and deeper areas are shaded. The shoreline is at $x = 0.0$, and the breaking line is at $x = 1.0$.

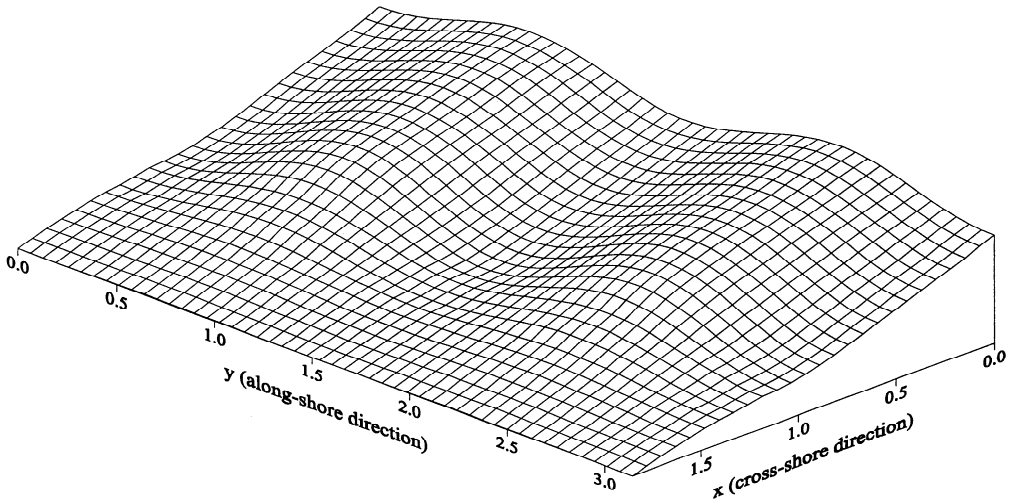

Figure 8. A 3-D view of the topographic perturbation (basic slope and perturbation amplitude have chosen arbitrarily) for $k = 3.0, r = 0.5, N = 0.01, \gamma = 0.02$, and $\alpha(x) = \text{const}$. The shoreline is at $x = 0.0$, and the breaking line is at $x = 1.0$.

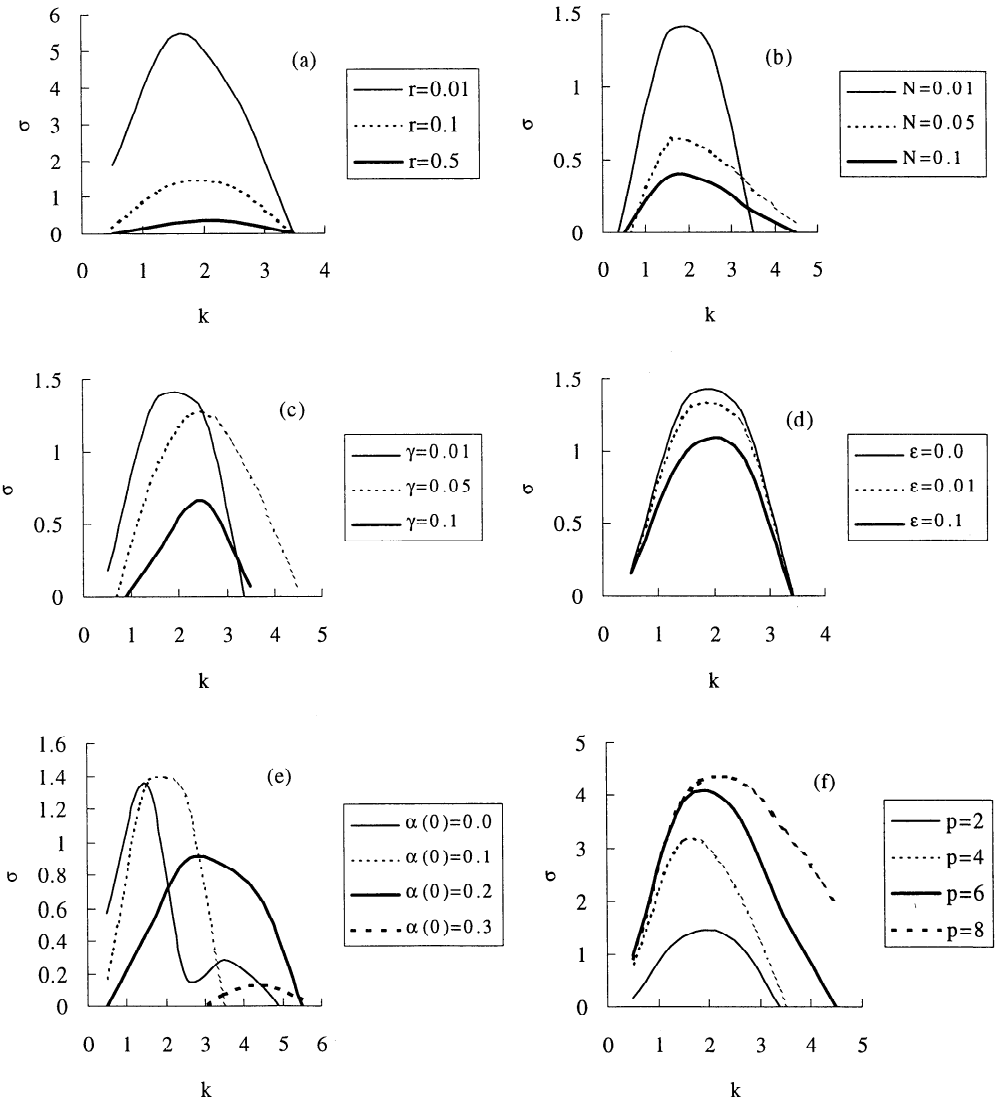

Figure 9. Effects of (a) friction r, (b) momentum diffusion N, (c) morphodynamic diffusion γ, (d) ϵ parameter, and (e) and (f) stirring function on crescentic pattern growth rates. Default parameters are $r = 0.1, N = 0.01, \gamma = 0.02, \epsilon = 0.01, \alpha(0) = 0.1$, and $p = 2$.

be verified by changing the value of the previously defined coefficient ϵ. Figure 9d shows that the adoption of relatively small values ($\epsilon = 0.01$) results in an instability curve that does not differ much ($< 2\%$) from $\epsilon = 0$. This is because the instability is on a morphological scale that is much larger than the hydrodynamical one so that the fluid adjusts instantaneously to the topographic changes. However, differences appear, though primarily more in the magnitude of the growth rate than in the wavelength, when comparable values are used for the morphological and hydrodynamical timescale (i.e., $\epsilon = 0.1$). Figures 9e and 9f are instead related to the sensitivity of the instability toward the parameterization of the stirring function. The usual form considered through the simulations is given by a quadratically increasing expression with a small nonzero value at the shoreline ($\alpha(0) = 0.1$). Variations in the shoreline value are shown in Figure 9e and, intriguingly, indicate a dependency of a such value also on the spacing of the features. As expected, higher shoreline values of the stirring coefficient, and so tending toward a constant profile, result in smaller growth rates, and for values $\alpha(0) > 0.3$, no instability is present. As previously indicated, a quadratic expression has been used in order to describe the stirring coefficient throughout the surf zone. The use of other exponents, here indicated with the letter p, results in strong variations in the growth rates which increase with higher powers (Figure 9f). The variation of the stirring coefficient profile offshore of the breaking line has also been investigated by using a constant value (equal to the one at the breaking line) or exponentially decreasing function. Results indicate that the growth rates are independent from the variation of the stirring function profile offshore of the breaking line.

5.2. Giant Cusp Pattern

Surprisingly, when the breaker line variations due to the perturbations in the water level and in the topography are included, the model does not predict any instability in the case of a constant stirring function. This is the case also for the other choices of the stirring function that for fixed breaker line produced the growth of the giant cusp pattern (like those exponentially decaying from the shoreline). Therefore, the movement of the breaker line inhibits the formation of the giant cusp pattern.

In order to understand this behavior, the circulation produced by the giant cusp topography was investigated by solving the FOT problem in the case including breaker line variations. As can be seen in Figure 10, a strong onshore current is created over the transverse bars while rip currents appear in the troughs. So, the flow pattern is reversed with respect to the case where the breaker line is kept fixed (Figure 7), and the cross-shore flow component has now the same direction as the gradient in $\alpha(x)/D_0(x)$. Therefore, in accordance with the bottom evolution equation (21) the bottom perturbation tends to decay, as predicted by the stability analysis.

The flow reversal can be understood as follows. The transverse bars crossing the breaker line produce a wa-

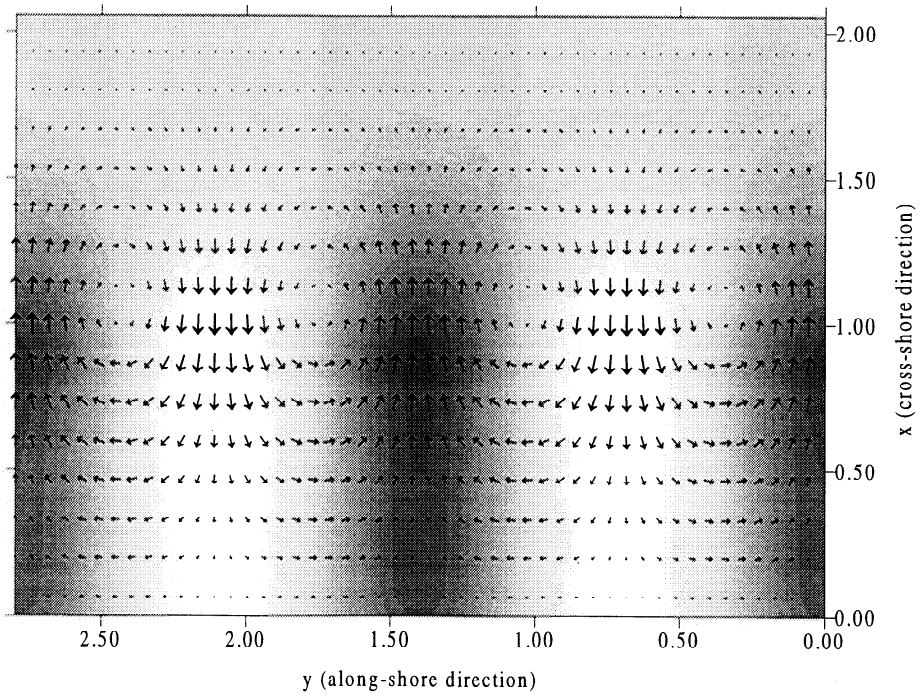

Figure 10. Linearized flow pattern over a fixed small-amplitude cuspate topography including the effect of the breaking line variation (solution of the linear FOT problem). Shoals are white, and deeper areas are shaded (shoreline at $x = 0.0$).

ter depth reduction, so that the breaker line moves seaward. This implies that the surf zone extension is increased and that waves that were not breaking in the basic state are now breaking in this new portion of surf zone. This produces a strong additional shoreward force that is capable of reversing the current. Similarly, an additional seaward force is created in between the bars. Figure 10 also shows how the onshore force due to the moving breaker line produces a strong increase (decrease) of setup over the bars (troughs).

Since the flow is onshore over the transverse bars, according to the predictions of section 3 this topographic pattern should grow if we assume an $\alpha(x)/D_0(x)$ function that increases seaward. However, the only unstable mode in this case is the crescentic pattern. The explanation for this is that any pattern that arises as a growing linear eigenmode has not only a positive growth rate but also (by definition) a uniform growth rate. According to the bottom evolution equation (21) this implies that h should be proportional to $|u\alpha\ d[\ln(\alpha/D_0)]/dx|$. This condition is not met in the case of the giant cusp pattern since the maximum sediment transport would be located where the perturbation is relatively small.

In order to make a comparison with the behavior of the giant cusp pattern we also include a similar FOT simulation for the crescentic pattern topography. The circulation and the free surface elevation are shown in Figure 11. There is an offshore flow over the shoals out of the surf zone and an onshore flow over the shoals within the surf zone. Comparison with Figure 4 reveals that this flow is almost the same as that observed in the case of a fixed breaker line. This is due to the fact that the crescentic pattern consists of alternating shoals and pools on both sides of the breaker line, so that the bathymetric perturbation vanishes at the breaker line. Therefore there is no perturbation of the breaker line, so the flow remains unchanged.

6. Discussion

Perturbations of the incident wave radiation stress induced by the topographic irregularities in a saturated surf zone can drive a cellular flow with a sediment transport pattern that is able to reinforce the bottom perturbations. In this way a positive feedback that leads to the coupled growth of nearshore large-scale bed forms and horizontal circulation with rip currents may occur. Basically, two instability modes may appear depending upon the form of the sediment stirring function $\alpha(x)$. The perturbation in water depth due to the instabilities produces a shift in the breaking line. Such an effect had not been accounted for in earlier similar studies. The present research has considered both fixed and varying breaking line cases.

For an α function with a significant increase seaward across the surf zone a "crescentic pattern" is generated. This consists of alternating shoals and pools on both sides of the breaking line, showing a mirroring effect. The associated flow pattern extends through the whole surf zone but has its maximum strength at the vortices developed around the breaking line. The alongshore wavelength of such features ranges between 3 and 5 times the surf zone width X_b and depends on the bot-

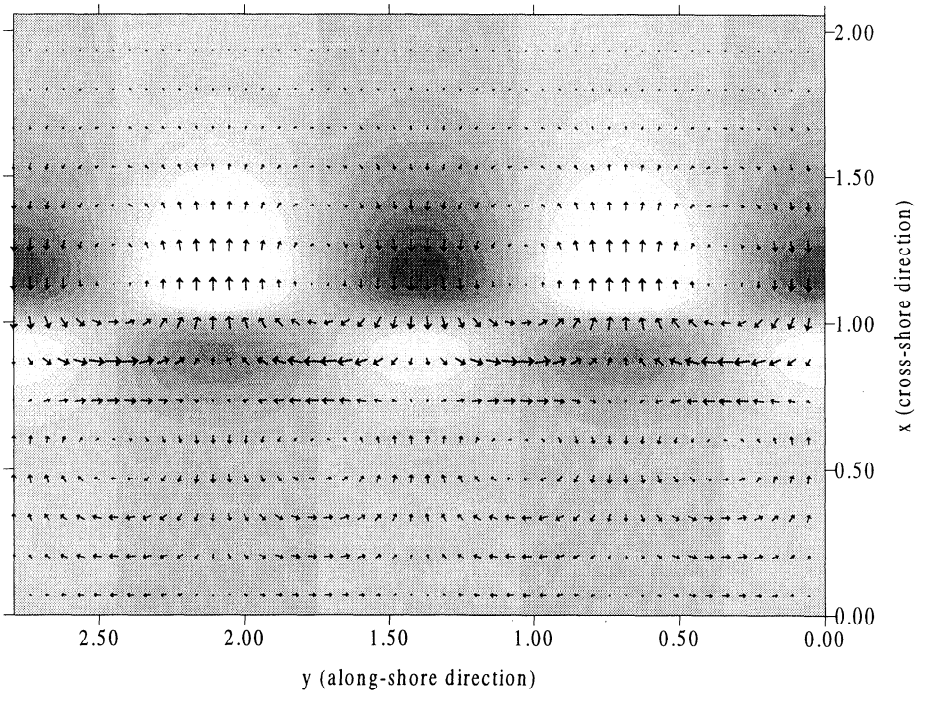

Figure 11. Linearized flow pattern over a fixed small amplitude crescentic bar topography including the effect of the breaking line variation (solution of the linear FOT problem). Shoals are white, and deeper areas are shaded (shoreline at $x = 0.0$).

tom friction, lateral momentum diffusion, and morphological diffusion, which have a damping effect. However, for realistic values of the damping parameters, growth rates are usually positive. This instability mode turns out to be essentially unaffected by the variations of the breaking line.

An interesting issue following these results is the shape of the crescentic pattern obtained in the present study, which is very similar to the one obtained by *Vittori et al.* [1999]. This is striking since their analysis aims to features outside the surf zone and the mean flow is generated by a very different mechanism (synchronous edge waves). However, a closer look reveals that this is not so surprising as they adopt the same sediment transport parameterization with a similar structure for the stirring function. Once again, we obtain a confirmation of something that can be unexpected at first sight: the coastal self-organization is often dominated by the sediment transport mode rather than by the mean hydrodynamics. This is clearly the case for the present investigation, where the emerging topography and the flow pattern depend ultimately on the distribution of wave stirring on the sediment. Another example is the orientation of oblique bars with respect to the coastline, upcurrent or downcurrent, which could sometimes depend on the $\alpha(x)$ function [*Falqués et al.*, 1999b].

An indication of the order of magnitude of the growth time of these features can be obtained from our morphological time scaling defined in (18). According to the data reported by *Antsyferov and Kos'yan* [1990] or by *Russell* [1993], 5 kg m^{-3} seems to be an appropriate order of magnitude of the suspended sediment concentration. Assuming a reference depth of 0.5 m, we then have $\bar{\alpha} \sim 10^{-3}$ m. The velocity scale can be calculated from the Froude number we used in the computations, $F = 0.12$, so that $U = 0.12\sqrt{g\beta X_b}$. Thus we find the estimate

$$T_{\mathrm{gro}} \sim 2.6 \times 10^3 \beta^{1/2} X_b^{3/2} \sigma^{-1} .$$

By assuming a nondimensional growth rate of $\sigma \sim 1$, a beach slope of $\beta \sim 0.05$, and a surf zone width of $X_b \sim 10$ m, the features, whose wavelength would be ~ 30 m, would grow significantly within some 5 hours. According to this, bed forms for $X_b \sim 5$ m, would grow within 1.8 hours, while very large bed forms for $X_b \sim 20$ m would not grow significantly until some 14 hours. These figures seem very sensible and perhaps suggest that the larger scale bed forms are not observed very often perhaps because of the fact that their growth time is longer than the typical time scale of the variability of wave conditions.

Alternatively, for an α function more or less constant or even decreasing seaward across the surf zone, a "giant cusp pattern" occurs if the breaking line is considered to be fixed. This consists of transverse bars attached to the shoreline and extending across the whole surf zone. The associated circulation has offshore flow over the crests and a return flow in between. The alongshore spacing between the bars is ~ 2 and 8 times X_b, typically somewhat shorter than the wavelength of the crescentic pattern. However, the breaking line displacement has a strong impact on this instability mode so that the associated flow pattern becomes reversed, the currents now being onshore at the crests and offshore at the troughs. Therefore, the circulation causes a damping of the bed forms whose growth becomes now inhibited. Which flow pattern results in the formation and development of giant cusps remains unclear, as is also testified to by the contradictions present in the literature (for a review, see, e.g., *Carter* [1988, p.120]). The possibility that the flow pattern providing the initial growth of the features differs from the one observed over finite amplitude features, where other effects like wave refraction [*Niedoroda and Tanner*, 1970] can become dominant, has to be considered.

The dependence of the instability modes upon the wave-stirring distribution suggests that crescentic patterns are likely to occur under relatively low wave conditions, while in principle, giant cusp patterns would be more likely under high wave conditions, when reflected long-period motion becomes significant. However, the varying breaking line effects rule out this latter possibility. Therefore we should conclude in agreement with *Carter* [1988] that the generation of giant cusps and more in general transverse bars, although observed in several circumstances, still remains something of an "enigma." Thus morphodynamic instabilities of an unbounded coast in case of normal wave incidence deserves further research.

The most obvious limitation of the present analysis is the assumption of regular waves, which results in a nonsmooth wave energy distribution. This introduces a singularity in the linear stability analysis and makes the mathematical procedure seem somewhat artificial. However, even with the common smooth energy distributions in the case of random waves, there are strong changes in the energy gradient at the location where the majority of the waves start to break. Therefore, even though there is no singularity in this case, there are strong variations in wave forcing with respect to the basic equilibrium in a narrow region. Thus the present idealized analysis seems to be representative of more realistic conditions.

Another limitation is the assumption that long-period motion is simply a stirring mechanism affecting the results only through α neglects its direct contribution to the hydrodynamics. Direct influence through the bottom shear stress (equation 13) is not expected to be qualitatively significant (see Figure 9). However, work is in progress to add long-period motion to the coupling of incident waves and sediment response to determine its effect on the morphodynamic instabilities discussed in this paper.

We should finally mention that the present study has been based on the assumption of a sediment transport

related only to the mean flow. The transport directly related to the waves should be also considered in future research through suitable parameterizations of undertow, wave asymmetry, etc.

The effect of incident wave refraction by the growing bed forms and the currents on the instability mechanism has been neglected. We do not think that this effect has a significant influence at the initial stage. However, as suggested by *Niedoroda and Tanner* [1970], it can be very important for the finite amplitude development of these features. This requires a nonlinear stability analysis, which is now under way. This kind of study of the finite amplitude evolution will also allow for the investigation of a different sediment transport, nonlinear in the mean flow. This will permit checking of the robustness of the crescentic pattern, gaining of new insight into the giant cusp pattern, and looking for possible subcritical finite amplitude instabilities.

Appendix A

In this appendix we show the link between the sediment transport parameterization described through (12) and other already accepted models based on an energetics approach. *Bowen* [1980] applied the *Bagnold* [1963] energetics equation to the case of a sinusoidal wave velocity and a much smaller mean flow and showed that the net sediment transport rate for both suspended and bedload transport takes the same form as (12). In particular, the suspended sediment transport rate takes the form

$$q = \frac{16\varepsilon_s c_f \rho}{3\pi w}\left(uU_0^3 + \frac{\beta}{5w}U_0^5\right),$$

where ε_s is the suspended sediment transport efficiency, c_f is the drag coefficient, ρ is the water density, w is the settling velocity, β is the slope, U_0 is the maximum wave orbital velocity, and u is the steady current. A comparison between such a formulation and that given in (12) implies that

$$\alpha(x) = C_1 U_0^3 \quad \gamma(x) = -C_1 \frac{U_0^5}{5w}$$

where $C_1 = 16\varepsilon_s c_f \rho/3\pi w$.

A simple model of wave velocities under normally incident shallow water waves provides a form for the cross-shore dependence of these functions $\alpha(x)$ and $\gamma(x)$. If we assume shoaling waves out of the surf zone and depth limited waves inside the surf zone with $H = \gamma_b D$, we obtain

$$U_0^2 = \begin{cases} C_2 x^{-3/2} & D > D_b \\ C_2 x & D < D_b \end{cases}$$

where: $x = D/D_b$ and $C_2 = g\gamma_b^2 D_b/4$. Thus obtaining the expression for the variation of the maximum orbital velocity U_0 thus of $\alpha(x)$ and $\gamma(x)$ with the offshore distance is possible. In fact, outside the surf zone

$$\alpha(x) = C_1 C_2^{3/2} x^{-9/4} \quad \gamma(x) = -\frac{C_1}{5w} C_2^{5/2} x^{-15/4},$$

while inside the surf zone:

$$\alpha(x) = C_1 C_2^{3/2} x^{3/2} \quad \gamma(x) = -\frac{C_1}{5w} C_2^{5/2} x^{5/2}.$$

These are the functions of x that have been modeled in this paper.

The case of $\alpha(x)$ and $\gamma(x)$ increasing toward the shoreline is related to the possibility of an environment dominated by the presence of edge wave motions. The edge wave theory is already well established [*Eckart*, 1951 ; *Ursell*, 1952] and for the present purposes it is important to note only that a standing edge wave in shallow water has a velocity potential given by

$$\Phi = \frac{g a_n}{\omega} L_n(2kx) e^{-kx} \cos ky \cos \omega t,$$

where a_n is the amplitude of order n, ω is the frequency, $L_n(2kx)$ is the Laguerre polynomial of order n, x and y are the horizontal coordinates in the offshore and alongshore direction, t is the time, and k is the long-shore wavenumber of the edge wave. The cross-shore orbital velocity field is given by the gradient of the velocity potential, and it results in a cross-shore profile of the form

$$u_*(x) = -\frac{\partial}{\partial(kx)}\left[L_n(2kx)\, e^{-kx}\right].$$

In nature one would expect to find the coexistence of edge waves characterized by different modes and wavelengths. For example, Figure 12 shows the effect of superimposing the velocity squared of the first seven modes of an edge wave of arbitrary wavelength. The rapid increase toward the shoreline is at least qualitatively modeled by the exponential forms used in the simulations in this paper.

For suspended sediment transport the function α in (12) models the cross-shore profile of the depth-integrated mean suspended sediment concentration. The

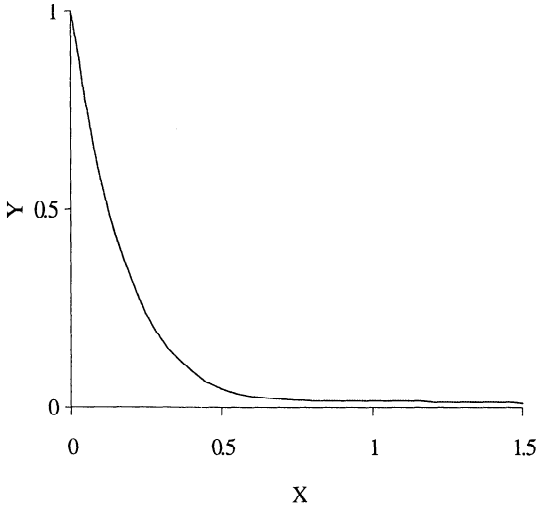

Figure 12. The sum of squares of the cross-shore velocities (Y) for the first seven edge wave modes on a linear slope (arbitrary units; X indicates the cross-shore direction).

relatively small number of published observations of mean concentration in the nearshore zone confirm that this cross-shore profile can take any of the qualitatively different forms that have been used in this study. *Antsyferov and Kos'yan* [1990] show measurements from a natural beach under "relatively constant small swell" (estimated breaker height around 1 m), where mean concentrations increase seaward from near zero at the shoreline, reach a maximum at the breakpoint, and then decay farther seaward. This profile shape is qualitatively similar to the form of α that we have found to create crescentic topography (figure 4). On the other hand, observations described by *Hwang et al.* [1996], from a beach of mild slope and offshore wave heights of between 1.6 and 2.2 m, show almost constant concentration through the surf zone, a form found to create giant cusp topography (figure 7). The observations of *Russell* [1993], for a breaker height in excess of 3 m, suggest that during storm conditions the concentration can even increase toward the shoreline, a form that could potentially create giant cusp topography.

Breaking incident waves alone would be expected to result in concentrations that decrease toward the shore; the simple model of the stirring effect of breaking wave currents described here is in fair agreement with the observations of *Antsyferov and Kos'yan* [1990]. However, waves reflected at the beach would have significant amplitude at the shoreline. There is strong evidence that long-period reflected wave height and velocity increase approximately linearly with breakpoint wave height [*Guza and Thornton*, 1982; *Huntley et al.*, 1993]. Thus the cross-shore concentration profiles observed by *Hwang et al.* [1996] and *Russell* [1993] for larger incident waves heights may be the result of the addition of significant long wave stirring, with a profile that would generally increase toward the shoreline. In fact *Russell* [1993] shows that long wave motion was dominant for his observations from the inner surf zone.

Appendix B

In this appendix we derive an integral identity and an inequality that are useful to show some of the properties of the solutions of the FOT equation (26) (flow over topography problem) in case of a fixed breaker line. To this end, let us multiply this equation by $D_0 u$ and choose two arbitrary cross-shore locations in the surf zone $1 \geq x_2 > x_1 \geq 0$ where the cross-shore velocity vanishes:

$$u(x_1) = u(x_2) = 0.$$

Then integration by parts leads to

$$\int_{x_1}^{x_2} \frac{\mu_y}{D_0}\left[\frac{\partial}{\partial x}(D_0 u)\right]^2 dx + \frac{1+m}{1+3m}k^2 \int_{x_1}^{x_2} \mu_x D_0 u^2\, dx = \frac{2s}{1+3m}k^2 \int_{x_1}^{x_2} D_0 u \frac{\partial h}{\partial x}\, dx \quad .$$

If both cross-shore positions were out the surf zone, $x_2 > x_1 \geq 1$, one then would obtain

$$\int_{x_1}^{x_2} \frac{\mu_y}{D_0}\left[\frac{\partial}{\partial x}(D_0 u)\right]^2 dx + k^2 \int_{x_1}^{x_2} \mu_x D_0 u^2\, dx = 0\,.$$

Since $\mu_x, \mu_y, D_0 > 0$, it then follows that $u(x) = 0$ for $x_2 \geq x \geq x_1$. By taking $u(\infty) = 0$ and by choosing $x_2 \to \infty$, we then have $u(x) = 0$ for $x \geq x_2$. Finally, by continuity, x_1 can be lowered to the breaker line $x = 1$. Therefore either $u(x) = 0$ for all $x \geq 1$ or $u(x) \neq 0$ for all $x \geq 1$. Another possibility would be $x_2 > 1 \geq x_1 \geq 0$ with $x_2 \to \infty$. In this case we get

$$\int_{x_1}^{\infty} \frac{\mu_y}{D_0}\left[\frac{\partial}{\partial x}(D_0 u)\right]^2 dx + k^2 \frac{1+m}{1+3m} \int_{x_1}^{1} \mu_x D_0 u^2\, dx + k^2 \int_{1}^{\infty} \mu_x D_0 u^2\, dx = \frac{2s}{1+3m}k^2 \int_{x_1}^{1} D_0 u \frac{\partial h}{\partial x}\, dx\,.$$

Therefore we conclude that

$$\int_{x_1}^{x_2} D_0 u \frac{\partial h}{\partial x}\, dx > 0 \qquad \text{(B1)}$$

whenever $u(x_1) = 0$ and either $u(x_2) = 0$ or $x_2 = 1$.

Appendix C

The model equations in case of a fixed breaker line presented in section 2 are now extended to allow for a variable breaker line. Since the position of the breaking line $x = X_b$ is defined by the condition

$$\gamma_b D(X_b) = H_b\,, \qquad \text{(C1)}$$

where H_b is the wave height and $D(x)$ is the total water depth, the perturbations in water depth due to the instability result in a perturbation of the breaking line, $\Delta X_b(y,t)$. To first order in the perturbations, equation (C1) reads

$$\gamma_b\left[D_0(X_b) + \eta(X_b,y,t) - h(X_b,y,t) + D_{0x}(X_b)\,\Delta X_b(y,t)\right] = H_b\,,$$

so that

$$\Delta X_b = -\frac{\eta(X_b,y,t) - h(X_b,y,t)}{D_{0x}(X_b)} \qquad \text{(C2)}$$

as $H_b = \gamma_b D_0(X_b)$ and where X_b is the position of the breaker line in the basic state. Notice that since the depth perturbations are assumed to be infinitesimal, the gradient of total water depth, $D_{0x} + \eta_x - h_x$, is always positive, and the assumption of $H = \gamma_b D$ does not produce any spurious wave amplitude increase shoreward.

As we will see, when the breaking line moves from $x = X_b$ to $x = X_b + \Delta X_b$, there is an unbalanced zero-order term in the cross-shore momentum equation. This term is nonvanishing only in an infinitesimal interval of ΔX_b width so that the resulting contribution is first order and should be considered for the stability analysis. The procedure is as follows. By inserting the radiation stress (equation (3)) and the expresion of the wave energy (equation (11)) in the governing equations (1), the x momentum balance to first order reads

$$\frac{\partial u}{\partial t} = -g\frac{\partial(\eta_0+\eta)}{\partial x} - \frac{3}{8}g\gamma_b^2\frac{\partial(D_0+\eta-h)}{\partial x} + \Theta_x\,, \qquad 0 < x < X_b + \Delta X_b\,, \quad \text{(C3)}$$

within the surf zone, and

$$\frac{\partial u}{\partial t} = -g\frac{\partial(\eta_0+\eta)}{\partial x} + \Theta_x\,, \quad X_b + \Delta X_b < x\,, \quad \text{(C4)}$$

out of the surf zone, where it is assumed that there are no gradients in the radiation stress. The dissipation terms (friction and viscosity) are indicated by Θ_x, and η_0 and D_0 are the free surface elevation and the total depth in the basic state (zero-order). We have assumed an alongshore position where $\Delta X_b > 0$. The opposite case can be treated in a similar manner. The momentum balance in the basic state then reads

$$0 = -g\frac{\partial(\eta_0)}{\partial x} - \frac{3}{8}g\gamma_b^2\frac{\partial(D_0)}{\partial x} \quad , \quad 0 < x < X_b\,, \quad \text{(C5)}$$

within the surf zone, and

$$0 = -g\frac{\partial(\eta_0)}{\partial x} \quad , \quad X_b < x \quad \text{(C6)}$$

out of the surf zone. By substracting the zero-order equations from (C3)-(C4) we then obtain

$$\frac{\partial u}{\partial t} = -g\frac{\partial \eta}{\partial x} - \frac{3}{8}g\gamma_b^2\frac{\partial(\eta-h)}{\partial x} + \Theta_x\,, \qquad 0 < x < X_b\,, \quad \text{(C7)}$$

$$\frac{\partial u}{\partial t} = -g\frac{\partial \eta}{\partial x} - \frac{3}{8}g\gamma_b^2\frac{\partial(\eta-h)}{\partial x} + \Theta_x - \frac{3}{8}g\gamma_b^2\frac{\partial D_0}{\partial x}\,, \qquad X_b < x < X_b + \Delta X_b\,, \quad \text{(C8)}$$

$$\frac{\partial u}{\partial t} = -g\frac{\partial \eta}{\partial x} + \Theta_x\,, \quad X_b + \Delta X_b < x\,. \quad \text{(C9)}$$

The important fact in these equations is that the last right-hand side term in (C8) is zero order. After a similar development in the case where $\Delta X_b < 0$, the three equations can be written as a single one that reads

$$\frac{\partial u}{\partial t} + g\frac{\partial \eta}{\partial x} - \Theta_x - F_1 - F_2 = 0 \quad , \quad 0 < x < \infty\,. \quad \text{(C10)}$$

The first wave forcing term is

$$F_1 = \begin{cases} -\frac{3}{8}g\gamma^2\frac{\partial(\eta-h)}{\partial x} & 0 < x < X_b \\ 0 & X_b < x \end{cases}$$

and the second one is

$$F_2 = \begin{cases} -\frac{3}{8}g\gamma^2\frac{\partial D_0}{\partial x} & X_b < x < X_b + \Delta X_b \\ 0 & \text{otherwise} \end{cases}$$

in case where $\Delta X_b > 0$ and

$$F_2 = \begin{cases} +\frac{3}{8}g\gamma^2\frac{\partial D_0}{\partial x} & X_b + \Delta X_b < x < X_b \\ 0 & \text{otherwise} \end{cases}$$

in case where $\Delta X_b < 0$.

Assume now that the perturbations u, v, η, h, and ΔX_b are of order $\varepsilon \ll 1$. If we divide (C10) by ε and then make $\varepsilon \to 0$, all the terms will be of $O(1)$ except F_2/ε which will tend to ∞ but only in an infinitesimal interval of a width of order ε. We then get a Dirac δ, and the way to deal with it is to solve the differential equation (C10) in $(0, X_b)$ and in (X_b, ∞) (i.e., with $F_2 = 0$), with the restriction that the integral of the left hand side over the whole $(0, \infty)$ must vanish:

$$\int_0^\infty \frac{\partial u}{\partial t}\,dx + g\int_0^\infty \frac{\partial \eta}{\partial x}\,dx - \int_0^\infty \Theta_x\,dx + \frac{3}{8}g\gamma^2\int_0^{X_b}\frac{\partial(\eta-h)}{\partial x}\,dx - \int_{X_b-|\Delta X_b|}^{X_b+|\Delta X_b|} F_2\,dx = 0\,.$$

Since to first order in the perturbations

$$\int_{X_b-|\Delta X_b|}^{X_b+|\Delta X_b|} F_2\,dx \simeq -\frac{3}{8}g\gamma^2\frac{\partial D_0}{\partial x}(X_b)\,\Delta X_b\,,$$

we finally obtain

$$g(1+\frac{3}{8}\gamma^2)\eta|_{x=0} - \frac{3}{8}g\gamma^2 h|_{x=0} + \int_0^\infty \Theta_x\,dx = \sigma\int_0^\infty u\,dx \quad \text{(C11)}$$

as the integral condition on the eigensolution, where it has already been assumed that $u \sim e^{\sigma t}$ and where use of (C2) has been made.

This formulation has been implemented in the numerical model *morfo13* by just substituting the differential equation (C10) at the first collocation point with $x_i \geq X_b$ by the discrete version of the integral equation (C11). Very small sensitivity to $x_i - X_b$ has been observed.

Acknowledgments. This work is part of the SASME project, which is funded by the Commission of the European Union under contract MAS3 CT97-0081. This research was carried out while Giovanni Coco was in receipt of a grant from the University of Plymouth. Support from universities and colleagues during exchange visits between Universitat Politècnica de Catalunya and the University of Plymouth is gratefully acknowledged.

References

Antsyferov, S. M., and Kos'yan, R., Study of suspended sediment distribution in the coastal zone, *Coastal Engineering, 14*, 147-172, 1990.

Bagnold, R. A., Mechanics of marine sedimentation, in *The Sea,* edited by M. N. Hill, chap. 3, pp. 507-528, Wiley-Interscience, New York, 1963.

Bailard, A. J., An energetics total load sediment transport model for a plane sloping beach. *J. Geophys. Res., 86,* 10938-10954, 1981

Barcilon, A. I. and Lau, J. P., A model for formation of transverse bars, *J. Geophys. Res., 78,* 2656-2664, 1973.

Bowen, A. J., Simple models of nearshore sedimentation: Beach profiles and long-shore bars, in *The Coastline of Canada,* edited by S. B. McCann, *Pap. 80-10,* pp. 1-11, Geol. Surv. of Can., Otawa, 1980.

Bowen A.J., and Guza, R.T., Edge waves and surf beat, *J. Geophys. Res., 83,* 1913-1920, 1978.

Bowen, A. J., and Inman, D. L., Edge waves and crescentic bars, *J. Geophys. Res., 76,* 8662-8671, 1971.

Bowen, A. J., and Inman, D. L., Nearshore mixing due to waves and wave induced currents, paper presented at ICES Symposium on Physical Processes Responsible for dispersion of Pollutants in the Sea, Aarkus, 1972.

Carter, R. W. G. *Coastal Environments,* Academic, San Diego, California, 1988.

Christensen, E. D., R. Deigaard, and J. Fredsøe, Sea bed stability on a long straight coast, paper presented at 24th International Conference on Coastal Engineering, Am. Soc. of Civ. Eng., Kobe, 1994.

Coco, G., Huntley, D. A., and O'Hare, T. J., Beach cusp formation: Analysis of a self-organisation model, paper presented at Coastal Sediments '99, Am. Soc. of Civ. Eng., Long Island, 1999a.

Coco, G., O'Hare, T. J., and Huntley, D. A., Beach cusps: A comparison of data and theories for their formation, *J. Coastal Res., 15,* 741-749, 1999b.

Deigaard R., Drønen N., Fredsøe J., Jensen J.H. and Jørgensen M.P., A morphological stability analysis for a long straight barred coast, *Coastal Engineering, 36,* 171-195, 1999.

Eckart, C., Surface waves in water of variable depth, *Wave Rep. 100,* 99 pp., Scripps Inst. Oceanogr., Univ. of Calif., La Jolla, 1951.

Falqués, A., A note on the Barcilon and Lau model for transverse bars, *Revista de Geofísica, 47,* 191-195, 1991.

Falqués, A., Montoto, A. and Iranzo, V., Bed-flow instability of the longshore current, *Cont. Shelf Res., 16,* 1927-1964, 1996a.

Falqués, A., Montoto, A. and Iranzo, V., Coastal morphodynamic instabilities, paper presented at 25th International Conference on Coastal Engineering, Am. Soc. of Civ. Eng., Orlando, 1996b.

Falqués, A., Montoto M. and Vila D., A note on hydrodynamic instabilities and horizontal circulation in the surf zone, *J. Geophys. Res., 104,* 20605-20615, 1999a.

Falqués, A., Ribas, F., Larroudé, P., and Montoto, A., Nearshore oblique bars: Modelling versus observations at the Truc Vert Beach, paper presented at River, Coastal and Estuarine Morphodynamics, Int. Assoc. of Hydr. Res. Symposium, Genova, 1999b.

Guza, R. T. and Thornton, E. B., Swash oscillations on a natural beach, *J. Geophys. Res., 87,* 483-491, 1982.

Hino M., Theory on formation of rip-current and cuspidal coast, paper presented at 14th International Conference on Coastal Engineering, Am. Soc. of Civ. Eng., Copenhagen, 1974.

Holman, R. A. and Bowen, A. J., Bars, bumps, and holes: models for the generation of complex beach topography, *J. Geophys. Res., 87,* 457-468, 1982.

Horikawa K. (Ed.), Nearshore dynamics and coastal processes, Univ. of Tokyo Press, Tokyo, 1988.

Hunter R. E., Clifton H. E. and Phillips R. L., Depositional processes, sedimentary structures, and predicted vertical sequences in barred nearshore systems, southern Oregon coast, *J. Sedimentary Petrology, 82,* 711-726, 1979.

Huntley, D. A., M. Davidson, P. E. Russell, Y. Foote and J. Hardisty, Long waves and sediment movement on beaches: recent observations and implications for modelling, *J. Coastal Res., 15,* 215-229, 1993.

Hwang, C., L. Tsai, P. Lin, and C. Tsai, Studies on the suspended concentration in the surf zone, paper presented at 25th International Conference on Coastal Engineering, Am. Soc. of Civ. Eng., Orlando, 1996.

Komar, P.D., Nearshore circulation and the formation of giant cusps, *Geol. Soc. Am. Bull., , 82,* 2643-2650, 1971.

Lippmann T. C. and Holman R. A., The spatial and temporal variability of sand bar morphology, *J. Geophys. Res., 95,* 11575-11590, 1990.

Longuet-Higgins, M. S., Longshore currents generated by obliquely incident sea waves, 1, *J. Geophys. Res., 75,* 6778-6789, 1970a.

Longuet-Higgins, M. S., Longshore currents generated by obliquely incident sea waves, 2, *J. Geophys. Res., 75,* 6790-6801, 1970b.

Mei C. C. *The applied dynamics of ocean surface waves,* World Sci., River Edge, N.Y., 1989.

Mulrennan, M. E., Ridge and runnel beach morphodynamics: An example from the central east coast of Ireland, *J. Coastal Res., 8,* 906-918, 1992.

Niedoroda, A. W., and W. F. Tanner, Preliminary study on transverse bars, *Mar. Geol., 9,* 41-62, 1970.

Russell, P. E., Mechanisms for beach erosion during storms, *Cont. Shelf Res., 13,* 1243-1266, 1993.

Shepard, F. P., *Submarine geology,* 557 pp., Harper Collins, New York, 1963.

Sonu, C. J., Collective movement of sediment in littoral environment, paper presented at 11th International Conference on Coastal Engineering, Am. Soc. of Civ. Eng., London, 1968.

Southgate, H. N., and L. M. Beltran, Self-organisational processes in beach morphology, in *Physics of Estuaries and Coastal Seas,* edited by J. Dronkers and M. B. A. M. Scheffers, pp. 409-416, A.A. Balkema, Rotterdam, 1998.

Ursell, F., Edge waves on a sloping beach, *Proc. R. Soc. London, Ser. A, 214,* 79-97, 1952.

Vittori, G., H. E. De Swart, and P. Blondeaux, Crescentic bedforms in the nearshore region, *J. Fluid Mech., 381,* 1999.

Werner, B. T., and Fink, T. M., Beach cusps as self-organized patterns, *Science, 260,* 968-971, 1993.

G. Coco, Complex System Laboratory, I.G.P.P. - Scripps Institution of Oceanography, University of California - San Diego, La Jolla, CA 92093-0225 (e-mail: coco@mawson.ucsd.edu)

A. Falqués, Departament de Física Aplicada, Universitat Politècnica de Catalunya, Jordi Girona 1-3, Barcelona 08034, Spain (e-mail: falques@fa.upc.es)

D. A. Huntley, Institute of Marine Studies, University of Plymouth, Drake Circus, Plymouth, PL4 8AA, England, U.K.(e-mail: dhuntley@plymouth.ac.uk)

(Received March 9, 1999; revised December 1, 1999; accepted March 22, 2000.)